Two-particle spectral function for disordered s-wave superconductors: Local maps and collective modes

Abhisek Samanta, Amulya Ratnakar, Nandini Trivedi, and Rajdeep Sensarma

Phys. Rev. B **101**, 024507 — Published 13 January 2020

DOI: 10.1103/PhysRevB.101.024507

Two-particle spectral function for disordered s-wave superconductors: local maps and collective modes

Abhisek Samanta[1],* Amulya Ratnakar[2], Nandini Trivedi[3], and Rajdeep Sensarma[1]†
1. Department of Theoretical Physics, Tata Institute of Fundamental Research, Mumbai 400005, India.
2. UM-DAE Centre for Excellence in Basic Sciences, Mumbai University, Mumbai, India
3. Physics Department, The Ohio State University, Columbus, Ohio, USA 43201

We make the first testable predictions for the *local two-particle* spectral function of a disordered s-wave superconductor, probed by scanning Josephson spectroscopy (sjs), providing complementary information to scanning tunneling spectroscopy (sts). We show that sjs provides a direct map of the local superconducting order parameter that is found to be anticorrelated with the gap map obtained by sts. Furthermore, this anticorrelation increases with disorder. For the momentum resolved spectral function, we find the Higgs mode separates from the continuum at arbitrarily small disorder and appears as a non-dispersive subgap feature at low momenta, spectrally separated from phase modes for all disorder strengths. The amplitude-phase mixing remains small at low momenta even when disorder is large. Remarkably, even for large disorder and high momenta, the amplitude-phase mixing oscillates rapidly in frequency and hence does not significantly affect the purity of the Higgs and phase dominated response functions.

I. INTRODUCTION

Superconductivity, characterized by a macroscopic complex wavefunction of Cooper pairs, can be destroyed along two distinct routes: (a) by reducing the amplitude of the wavefunction to zero, as observed in conventional clean superconductors at T_c, where Cooper pairs break apart, or (b) by disordering the phase of the wavefunction, while keeping the pairing amplitude finite, as seen in strongly interacting [1–3], or in strongly disordered superconductors[4–7].

There is strong experimental[8–10] and theoretical [5–7,11,12] evidence that the destruction of superconductivity in thin films at high disorder [13–15] is driven by loss of phase coherence of Cooper pairs, which continue to exist through the superconductor to insulator transition. The low energy excitations of this system are the dynamical fluctuations of the amplitude (Higgs) and phase (Goldstone mode) of the complex order parameter. While the Higgs mode plays an important role in theory of fundamental particles, and has been observed in recent experiments, in superconductors it has been studied experimentally using optical[16] and Raman[17] spectroscopy. It has also been studied in neutral ultracold atomic systems[18]. In disordered superconductors, recent experiments[10] have interpreted low energy optical absorption as indicative of absorption by Higgs modes.

While the claim of observing pure amplitude Higgs modes in ultracold atoms is firmer, there are two main issues that prevent current experiments on quantum materials from reaching similar unambiguous conclusions: (a) The materials are inherently disordered, and it is not clear to what extent the low energy absorption can be separated into pure phase and amplitude (Higgs) modes in systems with broken translational symmetry. (b) The experiments currently do not have direct access to a spatial map of the inhomogeneous superconducting order parameter in the disordered systems. In this paper, we use a systematic study of the evolution of collective modes with disorder to address these key questions.

In this work, we use a functional integral approach[19] non-perturbative in both interaction and disorder strength to trace the evolution of the two-particle collective spectrum of a disordered attractive Fermi Hubbard model. We present for the first time the full momentum and frequency dependence of the disorder averaged spectral function as well as spectral function maps in real space for a particular disorder realization. Our spectral function maps at large disorder show strong correlation between superconducting patches and regions with large low energy pair spectral weight, which are found to be anti-correlated with regions of large local single particle gap. We thus make testable predictions for scanning tunneling[20] and scanning Josephson spectroscopies[22].

Our theoretical approach allows us to separate the contribution of the amplitude (Higgs) modes, phase modes and the amplitude-phase mixing. We find that the local response is dominated by the phase modes, while the Higgs and amplitude-phase mixing contributions play a subdominant role. An intriguing feature of the spatial maps of the amplitude-phase mixing contribution is its oscillatory nature over length scales much shorter than the superconducting patches. Since local probes average the response over a few lattice spacings, we expect the mixing not to be important in determining experimental quantities.

The momentum-dependent spectral functions show two features important for understanding experiments: (a) At arbitrarily low disorder, the Higgs mode at zero momentum shifts from its clean case value at the threshold of the two particle continuum to a value within the two particle gap. The shift in the energy of the Higgs mode is non-perturbative in disorder, while the spectral weight in this subgap mode vanishes smoothly in the clean limit. At low momenta, this mode is non-dispersive and spectrally separated from the phase modes. Disorder thus makes the Higgs mode visible to experiments. (b) The amplitude-phase mixing at higher momenta show a dramatic evolution with disorder. At low disorder it is predominantly of one sign, while at larger disorder, it oscillates and changes sign rapidly with frequency. Thus, at high disorder, temperature or finite resolution broadening of spectroscopic probes will wash-out the effects of amplitude-phase mixing, a result that is rather counter-intuitive. Our work makes testable predictions for experiments and provides a bridge between microscopic models that start with fermionic degrees of freedom[5,6] and effective bosonic models[4,23].

The paper is organized in the following way: In section II, we describe the model Hamiltonian used to study disordered superconductors and our functional integral based approach to calculate the two particle spectral functions. Section III describes the features of the local pair spectral function maps while Section IV describes the features of the disorder averaged spectral function in momentum space, before we conclude in Section V with the key features of our calculations.

II. MODEL AND METHODS

We analyze the behavior of the disordered attractive Hubbard model on a square lattice using an inhomogeneous self-consistent functional integral approach. The Hamiltonian is given by:

$$H = -t \sum_{\langle rr' \rangle \sigma} c^{\dagger}_{r\sigma} c_{r'\sigma} - U \sum_{r} n_{r\uparrow} n_{r\downarrow} + \sum_{r} (v_r - \mu) n_r \quad (1)$$

where $c^{\dagger}_{r\sigma}(c_{r\sigma})$ is the creation (annihilation) operator for electrons with spin σ on site r, and μ is the chemical potential. t is the nearest-neighbour hopping, and U is the attractive interaction leading to Cooper pairing. Here, v_r is a random potential, drawn independently for each site from a uniform distribution of zero mean and width V, where V sets the scale of disorder. This model has been studied earlier within a spatially inhomogeneous Bogoliubov de-Gennes (BdG) mean field theory[5], which introduces the static local Cooper pairing field $\Delta_0(r) = -U\langle c^{\dagger}_{r\uparrow} c^{\dagger}_{r\downarrow}\rangle$ and the Hartree shift $\xi_0(r) = U\langle c^{\dagger}_{r\sigma} c_{r\sigma}\rangle$. This inhomogeneous mean field theory treats disorder exactly and obtains a large number of site-dependent mean fields self-consistently. The BdG theory also yielded the earliest indications that the single particle gap remains finite through the superfluid-insulator transition.

Here, we work in the functional integral formalism, where the BdG mean field theory can be obtained as a static but spatially inhomogeneous saddle point of the system. The partition function can be written in terms of the fermion fields $(\bar{f}_\sigma(r,\tau), f_\sigma(r,\tau))$ as

$$Z = \int D[\bar{f}_\sigma, f_\sigma] e^{-S[\bar{f}_\sigma, f_\sigma]}, \quad (2)$$

with the imaginary time (τ) action

$$S = \int_0^{\beta} d\tau \sum_{rr',\sigma} \bar{f}_\sigma(r,\tau) \left[\partial_\tau \delta_{rr'} + H^0_{rr'}\right] f_\sigma(r',\tau) - U \sum_r \bar{f}_\uparrow(r,\tau) \bar{f}_\downarrow(r,\tau) f_\downarrow(r,\tau) f_\uparrow(r,\tau) \quad (3)$$

where $\beta = 1/T$, T being the temperature of the system and $H^0_{rr'} = -t\delta_{\langle rr' \rangle} - (\mu - v_r)\delta_{rr'}$. Using Hubbard-Stratanovich auxiliary fields $\Delta(r,\tau)$ coupling to $\bar{f}_\uparrow(r,\tau)\bar{f}_\downarrow(r,\tau)$ and $\xi(r,\tau)$ coupling to $\bar{f}(r,\tau)f(r,\tau)$, and introducing the Nambu spinors $\psi^{\dagger}(r,\tau) = \{\bar{f}_\uparrow(r,\tau), f_\downarrow(r,\tau)\}$, we get

$$Z = \int D[\bar{f}_\sigma, f_\sigma] D[\Delta^*, \Delta] D[\xi] e^{-S_{eff}[\bar{f}_\sigma, f_\sigma, \Delta^*, \Delta, \xi]}, \quad (4)$$

with

$$S_{eff} = \int_0^{\beta} d\tau \sum_r \frac{|\Delta(r,\tau)|^2 + |\xi(r,\tau)|^2}{U} - \int d\tau d\tau' \sum_{rr'} \psi^{\dagger}(r,\tau) G^{-1}(r,\tau; r',\tau') \psi(r',\tau'), \quad (5)$$

$$\text{and} \quad G^{-1}(r,\tau;r',\tau') = \delta(\tau-\tau') \begin{pmatrix} -(\partial_\tau - \mu(r,\tau))\delta_{rr'} + t\delta_{\langle rr' \rangle} & -\Delta(r,\tau)\delta_{rr'} \\ -\Delta^*(r,\tau)\delta_{rr'} & -(\partial_\tau + \mu(r,\tau))\delta_{rr'} - t\delta_{\langle rr' \rangle} \end{pmatrix},$$

where $\mu(r,\tau) = \mu - v(r) + \xi(r,\tau)$. The static but spatially dependent saddle point profile, $\Delta(r,\tau) = \Delta_0(r)$ and $\xi(r,\tau) = \xi_0(r)$ to write the saddle point action S_0. This reproduce the BdG mean field theory, with the saddle point equations $\delta S_0/\delta\Delta_0(r) = 0$ and $\delta S_0/\delta\xi_0(r) = 0$, giving the BdG self-consistency equations at $T = 0$ (See Appendix A for details),

$$\Delta_0(r) = |U| \sum_n u_n(r) v^*_n(r), \quad (6)$$

$$\xi_0(r) = |U| \sum_n |v_n(r)|^2 \quad \text{and} \quad \langle n \rangle = \frac{2}{N_s} \sum_{n,r} |v_n(r)|^2, \quad (7)$$

where S_0 is the saddle point action. $\langle n \rangle$ is the average density of electrons in the system with N_s number of sites. Here $[u_n(r), v_n(r)]$ are the eigenvector of $G^{-1}(r, r', \omega)$ corresponding to eigenvalue $\omega - E_n$ and n runs over only positive eigenvalues ($E_n > 0$).

The main goal of this work is to understand the evolution of the quantum fluctuations in the system with disorder, with a focus on the low energy collective modes of the system. We first solve the BdG self-consistency equations (Eqn. 6 and 7) on a 24×24 square lattice with an interaction strength $U/t = 3$ and at an average fermion density $\rho = 0.875$. We also consider 15 disorder realizations for each disorder value. This provides the inhomogeneous saddle point of the disordered system.

Going beyond the saddle point approximation, we include (in Eqn. 5) the spatio-temporal fluctuations of the Δ field i.e.

$$\Delta(r,\tau) = (\Delta_0(r) + \eta(r,\tau))e^{i\theta(r,\tau)}, \tag{8}$$

where $\eta(r,\tau)$ is the amplitude and $\theta(r,\tau)$ is the phase fluctuation around the saddle point solution. Now we use a gauge transformation to get rid of the fluctuating phase of the Δ field (in Eqn. 5). This is achieved by transforming to a new fermion co-ordinate given by $\tilde{\psi}(r,\tau) = U^\dagger(r,\tau)\psi(r,\tau)$, where

$$U(r,\tau) = \cos\left(\frac{\theta(r,\tau)}{2}\right)\mathbb{I} + i\sin\left(\frac{\theta(r,\tau)}{2}\right)\sigma^z. \tag{9}$$

In this co-ordinate, the inverse of Nambu Green's function is given by $\tilde{G}^{-1} = U^\dagger G^{-1} U$, which can be written as

$$\tilde{G}^{-1}(r,\tau;r',\tau') = G_0^{-1}(r,\tau;r',\tau') + \mathcal{K}(r,\tau;r',\tau') \tag{10}$$

where G_0^{-1} is the saddle point inverse Green's function with $\Delta(r,\tau) = \Delta_0(r)$ and the fluctuations are encoded in $\mathcal{K}$, given by

$$\begin{aligned}\mathcal{K}(r,\tau;r',\tau') = \delta(\tau-\tau')\Big[&\left\{\frac{-i}{2}\partial_\tau\theta(r,\tau)\delta_{rr'} + t\left[\cos\left(\frac{\nabla\theta(r,r',\tau)}{2}\right) - 1\right]\delta_{\langle rr'\rangle}\right\}\sigma^z \\ &-it\sin\left(\frac{\nabla\theta(r,r',\tau)}{2}\right)\delta_{\langle rr'\rangle}\mathbb{I} - \eta(r,\tau)\delta_{rr'}\sigma^x\Big]\end{aligned} \tag{11}$$

where the lattice derivative for two nearest neighbour sites r and r' is given by $\nabla\theta(r,r',\tau) = \theta(r,\tau) - \theta(r',\tau)$.

Since the functional integral is quadratic in fermion fields, the fermions can now be integrated out (Eqn. 4) to obtain a nonlinear action written in terms of $\Delta_0(r)$, $\eta(r,\tau)$ and $\theta(r,\tau)$,

$$S = S_0 + \frac{1}{U}\int d\tau \sum_r \eta(r,\tau)^2 + \frac{2}{U}\int d\tau \sum_r \Delta_0(r)\eta(r,\tau) - \int d\tau d\tau' Tr\ln[1 + G_0\mathcal{K}] \tag{12}$$

where S_0 is the saddle point action and the Trace is over both Nambu and site indices. The resulting action is expanded upto quadratic order in η and θ to obtain the Gaussian action for the amplitude and phase fluctuations,

$$S_G = \sum_{rr'}\sum_{\omega_m} \begin{pmatrix} \eta(r,\omega_m) & \theta(r,\omega_m) \end{pmatrix} \begin{pmatrix} {D^{-1}}_{11}(r,r',\omega_m) & {D^{-1}}_{12}(r,r',\omega_m) \\ {D^{-1}}_{21}(r,r',\omega_m) & {D^{-1}}_{22}(r,r',\omega_m) \end{pmatrix} \begin{pmatrix} \eta(r',-\omega_m) \\ \theta(r',-\omega_m) \end{pmatrix}. \tag{13}$$

where $\omega_m = (2m)\pi/\beta$ is the Bosonic Matsubara frequency. We work in the amplitude and phase degrees of freedom rather than the "Cartesian" co-ordinates which mix these degrees of freedom, so that we can cleanly talk about Higgs and phase modes. The inverse propagator matrix D^{-1} is analytically continued to real frequencies. We note that we work directly in real frequencies and do not need to do numerical analytic continuation. Working at $T = 0$, here we present the formulae for the real frequency retarded inverse fluctuation propagators ${D^{-1}}_{\alpha\beta}(i,j,\omega)$ in terms of BdG eigenvalues and eigenfunctions.

$$D^{-1}{}_{11}(r,r',\omega) = \frac{1}{U}\delta_{rr'} + \frac{1}{2}\lim_{i\omega_m\to\omega+i0^+}\sum_{\omega_n} Tr^N\left[G_0(r,r',\omega_n)\sigma^x G_0(r',r,\omega_n+\omega_m)\sigma^x\right]$$
$$= \frac{1}{U}\delta_{rr'} + \frac{1}{2}\sum_{E_{n,n'}>0} f^1_{nn'}(r)f^1_{nn'}(r')\chi_{nn'}(\omega) \tag{14}$$

where Tr^N corresponds to Trace in Nambu space, and

$$f^1_{nn'}(r) = [u_n(r)u_{n'}(r) - v_n(r)v_{n'}(r)] \quad \text{and}$$
$$\chi_{nn'}(\omega) = \frac{1}{(\omega+i0^+ - E_n - E_{n'})} - \frac{1}{(\omega+i0^+ + E_n + E_{n'})}. \tag{15}$$

$$D^{-1}{}_{12}(r,r',\omega) = \frac{i}{4}\lim_{i\omega_m\to\omega+i0^+}(i\omega_m)\sum_{\omega_n} Tr^N\left[G_0(r,r',\omega_n)\sigma^z G_0(r',r,\omega_n+\omega_m)\sigma^x\right]$$
$$= -\frac{i\omega}{4}\sum_{E_{n,n'}>0} f^1_{nn'}(r)f^2_{nn'}(r')\chi_{nn'}(\omega) \tag{16}$$

where $f^2_{nn'}(r) = [u_n(r)v_{n'}(r) + v_n(r)u_{n'}(r)]$.

$$D^{-1}_{22}(r,r',\omega) = \tilde{D}_{dia}(r,r') + \omega^2\kappa(r,r',\omega) + \Lambda(r,r',\omega) \tag{17}$$

where the diamagnetic piece $\tilde{D}_{dia} = 2\sum_{\langle rr_1\rangle} S(r,r_1)$ for $r = r'$, $\tilde{D}_{dia} = -2S(r,r')$ when r and r' are nearest neighbours, and 0 otherwise, where $S(r,r') = \frac{t}{8}\sum_{\omega_n} Tr^N\left[G_0(r,r',\omega_n)\sigma^z\right] = \frac{t}{4}\sum_{E_n>0} v_n(r)v_n(r')$. The compressibility κ is given by,

$$\kappa(r,r',\omega) = \frac{1}{8}\lim_{i\omega_m\to\omega+i0^+}\sum_{\omega_n} Tr^N\left[G_0(r,r',\omega_n)\sigma^z G_0(r',r,\omega_n+\omega_m)\sigma^z\right]$$
$$= \frac{1}{8}\sum_{E_{n,n'}>0} f^2_{nn'}(r)f^2_{nn'}(r')\chi_{nn'}(\omega) \tag{18}$$

and the paramagnetic current-current correlator on the lattice, $\Lambda(r,r',\omega)$ is given by the expression,

$$\Lambda(r,r',\omega) = \sum_{\langle rr_1\rangle\langle r'r_2\rangle} J(r,r_1,r',r_2,\omega) - J(r,r_1,r_2,r',\omega) - J(r_1,r,r',r_2,\omega) + J(r_1,r,r_2,r',\omega)$$

where
$$J(r,r_1,r',r_2,\omega) = -\frac{t^2}{8}\lim_{i\omega_m\to\omega+i0^+}\sum_{\omega_n} Tr^N\left[G_0(r_2,r,\omega_n)G_0(r_1,r',\omega_n+\omega_m)\right]$$
$$= -\frac{t^2}{8}\sum_{E_{nn'}>0} f^3_{nn'}(r,r_1)f^3_{nn'}(r_2,r')\chi_{nn'}(\omega)$$

where $f^3_{nn'}(r,r') = [u_n(r)v_{n'}(r') - v_n(r)u_{n'}(r')]$.

We construct the inverse propagators in real space (continued to real frequency), invert the matrix to obtain the propagators $D_{\alpha\beta}(r,r',\omega)$. This leads to the spectral functions, $\mathcal{P}_{\alpha\beta}(r,r',\omega) = -\frac{1}{\pi}\text{Im}D_{\alpha\beta}(r,r',\omega)$, where

$$\mathcal{P}_{11}(r,r',\omega) = -\frac{1}{\pi}\text{Im}\langle\eta(r,\omega+i0^+)\eta(r',-\omega+i0^+)\rangle$$
$$\mathcal{P}_{12}(r,r',\omega) = -\frac{1}{\pi}\text{Im}\langle\eta(r,\omega+i0^+)\theta(r',-\omega+i0^+)\rangle$$
$$\mathcal{P}_{22}(r,r',\omega) = -\frac{1}{\pi}\text{Im}\langle\theta(r,\omega+i0^+)\theta(r',-\omega+i0^+)\rangle \tag{19}$$

i.e. $\mathcal{P}_{11}$ is the spectral density of amplitude fluctuations, $\mathcal{P}_{22}$ that of phase fluctuations and $\mathcal{P}_{12}$ is the amplitude-phase mixing term[24].

While η and θ are the natural choice of fluctuation coordinates, experimental probes couple to the fermion density or current, i.e. to $\Delta_0(r)e^{i\theta(r,\tau)} \sim i\Delta_0(r)\theta(r,\tau)$; e.g. Josephson spectroscopy can be understood in terms of coherent tunneling of Cooper pairs across a barrier. The standard formulation of Josephson current only considers the current carried by the condensate of Cooper pairs and hence is related to the square of the 1-particle anomalous Green's functions. However, when current carried by collective fluctuations is considered, the differential conductance (dI/dV) of Josephson spectroscopy has an additional term proportional

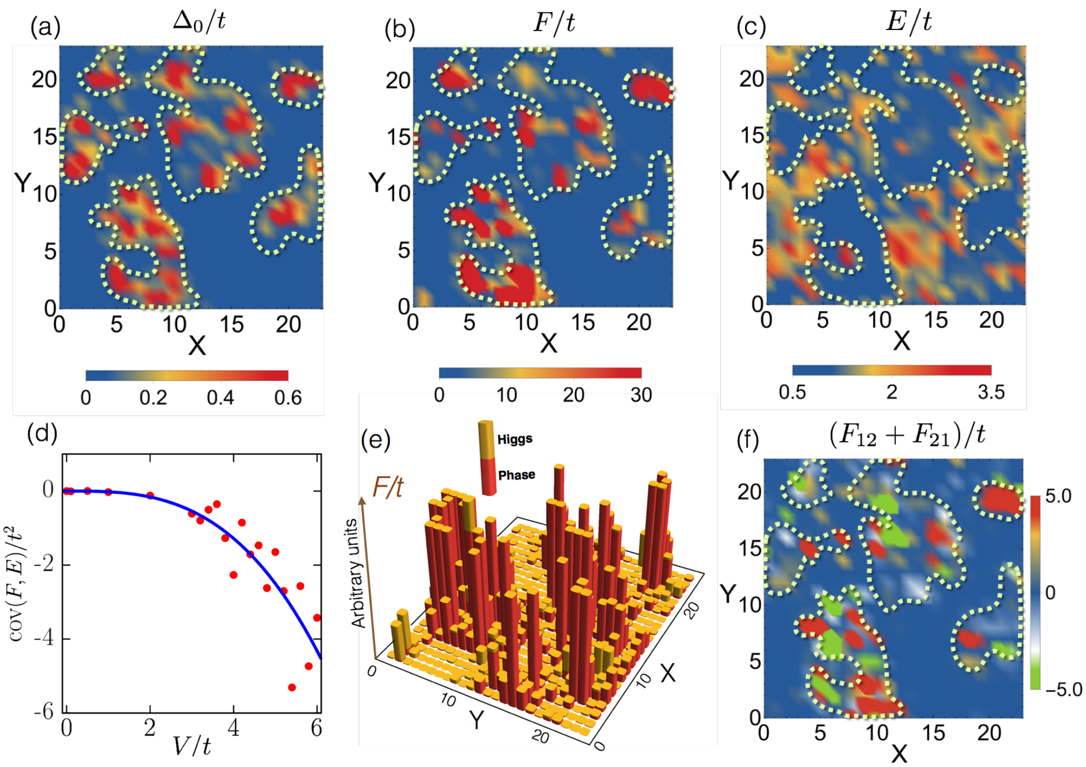

FIG. 1. Spatial maps for a particular disorder configuration at $V/t = 6$ showing strong correlation between (a) the local superconducting order parameter $\Delta_0(r)$ and (b) the frequency-integrated local 2-particle spectral weight $F(r)$. (c) Spatial map of the corresponding single particle gap $E(r)$ obtained from the local 1-particle density of states [See Appendix C for details]. Notice the strong anti-correlation between (c) and (b). (d) Covariance between $F(r)$ and $E(r)$, averaged over disorder realizations, as a function of disorder strength. The anti-correlation increases with disorder. (e): A bar map showing the relative weights of the Higgs (amplitude) and Goldstone (phase) modes in the two-particle spectral weight $F(r)$ shown in (b). The spectral weight at large disorder is dominated by the phase modes. (f) The integrated amplitude-phase cross-correlator $F_{12}(r) + F_{21}(r)$ corresponding to the configuration shown in (b). The mixing contribution shows regions with positive and negative values on a scale much smaller than the superconducting coherence length. Here, we present data with $U/t = 3$ on a 24×24 lattice, at an average fermion density $\rho = 0.875$.

to the spectral function of the Cooper pairs (2-particle spectral function)[25]. This is analogous to the STM (where electrons tunnel) measuring the electronic density of states. In strongly disordered superconductors, the current carried by collective fluctuations can be as large as the condensate contribution. The contribution of the fluctuations to the voltage derivative of the Josephson current is proportional to the pair spectral function $P(r, r', \omega) = \sum_{\alpha\beta} P_{\alpha\beta}(r, r', \omega)$, where $P_{11} = \mathcal{P}_{11}$, $P_{12}(r, r', \omega) = \Delta_0(r)\mathcal{P}_{12}(r, r', \omega)$, $P_{21}(r, r', \omega) = \Delta_0(r')\mathcal{P}_{21}(r, r', \omega)$ and $P_{22}(r, r'\omega) = \Delta_0(r)\Delta_0(r')\mathcal{P}_{22}(r, r', \omega)$.

We construct the pair correlation functions $P_{\alpha\beta}$ for each disorder realization. We note that for a given realization of disorder, translational symmetry is broken and the spectral function does depend on two co-ordinates r and r'; i.e. $P(r, r', \omega)$. We can rewrite this in relative and center of mass co-ordinates, $P(d, R, \omega)$ where $d = r - r'$ and $R = (r + r')/2$. Now, on averaging the data over disorder realizations, translational symmetry is restored. We then average over the center of mass co-ordinate R (which now gives a trivial volume factor) and express the disorder averaged spectral function as a function of relative coordinate only $P(d, \omega) = 1/N\langle\sum_R P(d, R, \omega)\rangle$, where N is the number of sites and $\langle\rangle$ indicates disorder average. Since this is a function of d only, momentum is a good quantum number for the disorder averaged pair spectral function. $P(q, \omega)$ is then the Fourier transform of $P(d, \omega)$. We note that in our formalism, the disorder averaging is done after calculating the relevant correlation function, and not at any intermediate stage.

We note that while the gaussian approximation provides a description of collective modes, it ignores the vortex excitations which finally drive the superfluid-insulator transition. The present formulation is inadequate very close to the transition, specially for quantities like superfluid stiffness, speed of sound, value of critical disorder. However, the gaussian approximation continues to provide an upper bound and captures the qualitative trends, which are the focus of this paper.

We will next study the evolution of pair spectral function, P both real and momentum space with disorder.

III. LOCAL PAIR SPECTRAL FUNCTION

At intermediate and large disorder, the system breaks up into superconducting and insulating islands[5]. STM measurements show evidence of strong spatial electronic inhomogeneity[20,21]. However, a direct access to the inhomogeneous superconducting order parameter is missing in these systems. We predict that the superconducting regions have large pair spectral weight and small single particle gaps. Our prediction can be experimentally tested by combining scanning tunneling with scanning Josephson spectroscopy data[22].

To study the spatial variation of the two particle spectral function $P(r, r', \omega)$, we consider its local part and integrate upto two particle continuum ($2E_{gap}$). We note that while E_{gap} is the gap to the single particle fermionic excitations, $2E_{gap}$ is the threshold for the continuum of 2-particle excitations. We restrict the integral to just below $2E_{gap}$ so that only contribution of collective modes is considered.

$$F(r) = 1/(2E_{gap}) \int_0^{2E_{gap}} d\omega P(r, r, \omega). \tag{20}$$

In Fig. 1(a) and (b), we show the local order parameter $\Delta_0(r)$ and the integrated local 2-particle spectral weight, $F(r)$ for a typical configuration at large disorder ($V/t = 6$). We notice the strong spatial correlation between regions with large $\Delta_0(r)$ and large $F(r)$. Although regions with small $\Delta_0(r)$ have small phase stiffness, these phase fluctuations do not contribute to the pair spectral function as $\Delta_0(r)$ is small in these regions. The integrated spectral weight can thus be used to experimentally map out the superconducting regions in the system. In Fig. 1(c), we plot the local single particle gap $E(r)$, obtained from peaks in the local one particle density of states for the same configuration [See Appendix C for details]. The maps in Fig. 1 (a) and (b) show strong spatial anti-correlation between regions with large $\Delta_0(r)$ or $F(r)$ and regions with large $E(r)$, i.e., large single particle gaps map out the insulating regions in the system. To track the evolution of this strong anti-correlation between $F(r)$ and $E(r)$, in Fig. 1(d), we plot the covariance of these quantities [See Appendix D for details], averaged over disorder configurations, as a function of V/t. The negative correlations increase with disorder, as the system breaks up into superconducting and non-superconducting regions.

The relative contribution of the Higgs channel (P_{11}), phase channel (P_{22}), and the amplitude-phase mixing ($P_{12} + P_{21}$) to the 2-particle spectral function is a key question of interest, especially in light of papers with contradictory claims on this topic[8,11,26,27]. To understand whether the spectral function is dominated by amplitude or phase fluctuations, in Fig. 1(e), we plot a bar on each site of the square lattice, the height of the bar being proportional to the integrated spectral weight on that site. For a visual representation, the phase and amplitude contributions are marked by different colours in each bar. We see that the local 2-particle spectral weight is dominated by the phase fluctuations, with the amplitude playing a sub-leading role. The mixing contribution, $F_{12} + F_{21}$ is plotted as a map in Fig. 1(f). P_{12} and P_{21} do not have the interpretation of a spectral weight and changes from positive to negative even within a single superconducting patch. Thus, although mixing contributions are similar in magnitude to Higgs contributions, we expect it to have a minimal impact on spatially-averaged responses.

IV. MOMENTUM AND ENERGY DEPENDENCE OF COLLECTIVE MODES

We now consider the Fourier transform of the disorder averaged spectral functions, $P_{\alpha\beta}(q, \omega) = \sum_{rr'} e^{iq\cdot(r-r')} P_{\alpha\beta}(r, r', \omega)$, to study the behaviour of the collective modes. In the optical conductivity the pair spectral function contributes to loop corrections, hence their effect cannot be spectrally resolved. A more direct momentum and frequency resolved measurement is possible with the recently developed M-EELS techniques[28].

First we study the amplitude contribution to the two particle spectral function in $q - \omega$ space. Fig. 2(a) -(d) shows the Higgs spectral function $P_{11}(q, \omega)$ with increasing disorder. For $V/t = 0$, a Goldstone mode exists, but the Higgs contribution to the spectral weight vanishes as $q \to [0, 0]$. The picture changes dramatically even in presence of a very weak disorder, $V/t \sim 0.05$. Here we show data for a weak disorder $V/t = 0.1$ in Fig. 2(b), where, in addition to the collective mode seen in the clean case, the Higgs spectral function develops an additional tail with finite weight at the zone center at an energy well below the two-particle continuum threshold. We emphasize that the location of the Higgs peak shifts by a finite amount from its value of $2E_{gap}$ in the clean case for an arbitrarily small disorder (Fig. 2(b)); this shift is therefore non-perturbative in the disorder strength, while the spectral weight in this subgap mode smoothly increases with disorder. The relatively flat dispersion of the Higgs peak suggests that these excitations gain energy by transforming from a propagating to a localized mode, and are pulled down from the edge of the two particle continuum.

To study the evolution of the Higgs mode, in Fig. 2(b)-(d) we plot the Higgs spectral function for increasing disorder, for $V/t = 0.1$(b), $V/t = 1.0$ (c) and $V/t = 3.0$ (d). The Higgs spectral function flattens and broadens with increasing disorder. We define the Higgs gap, ω_{higgs} as the lower threshold frequency at $q = 0$ where the Higgs mode appears and below which there is no Higgs spectral weight. We plot ω_{higgs} as a function of disorder and we find that it decreases monotonically with disorder (Fig. 2(i)) and becomes zero at a sufficiently strong disorder $V/t \sim 5.5$. We also observe a pile-up of low energy weight at the commensurate M point ($[\pi, \pi]$) at intermediate disorder of $V/t = 1.0$, indicating fluctuating pair-density waves, although there is no zero energy weight and static order is absent in the mean-field theory. We note that in presence of strong disorder, the collective mode structure in the amplitude sector is completely lost and it is dominated by the appearance of disorder induced flat modes (Fig. 2 (c) and (d)).

We now focus on the phase contribution to the spectral function $P_{22}(q, \omega)$ (Fig. 2 (e)-(h)). In a clean superconduc-

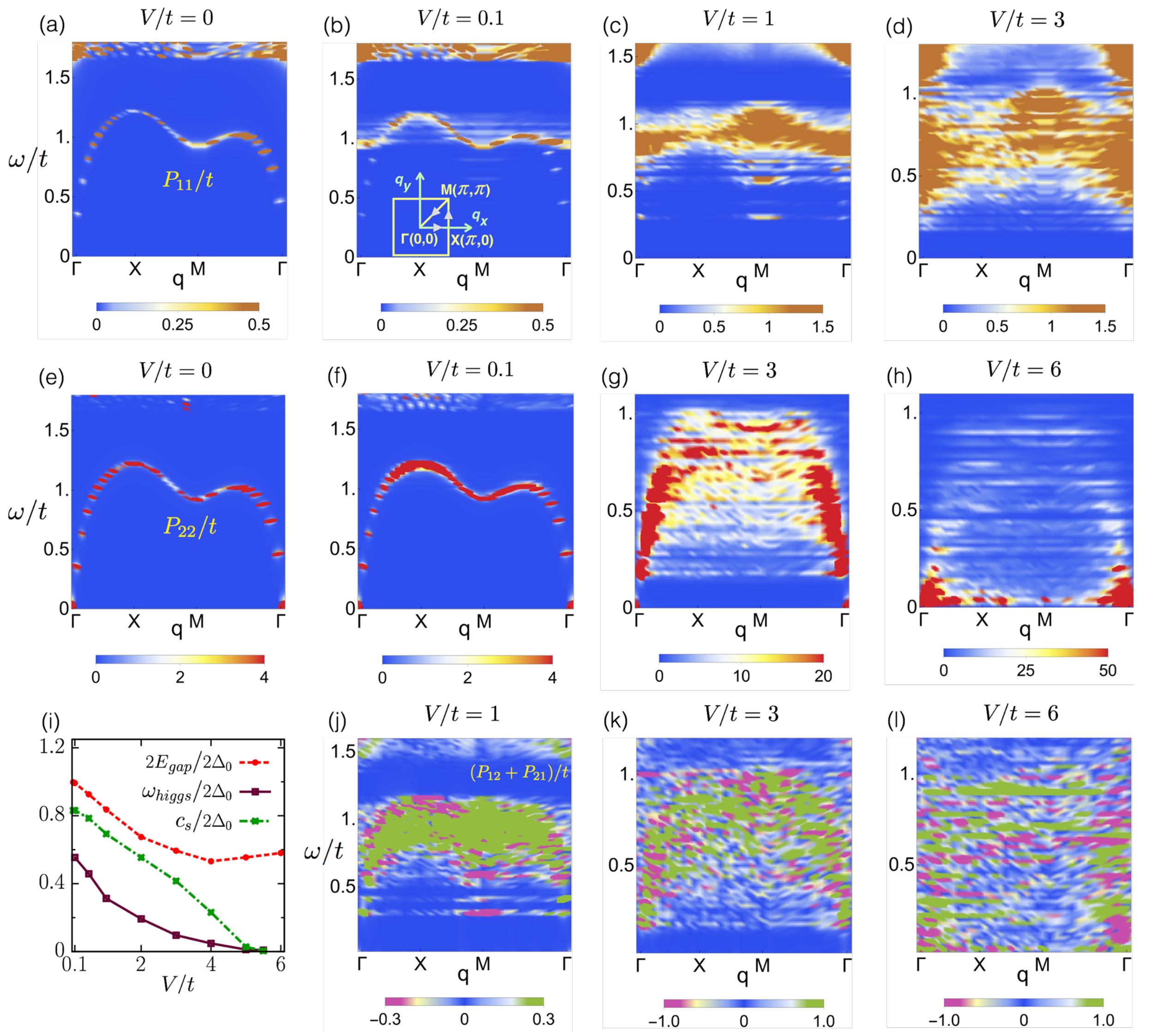

FIG. 2. (a)-(d): Density plot of Higgs spectral function $P_{11}(q, \omega)$ with increasing disorder: (a) $V/t = 0$ showing no weight at $q = 0$; (b) weak disorder $V/t = 0.1$ starts showing finite $q = 0$ weight of the Higgs mode; (c) $V/t = 1$ and (d) $V/t = 3$. (e)-(h): Density plot of Goldstone or phase spectral function $P_{22}(q, \omega)$ for (e) $V/t = 0$, (f) $V/t = 0.1$, (g) $V/t = 3$, and (h) $V/t = 6$. Note the stability of dispersive modes up to large disorder strength. For $V/t = 0.1$, note the absence of phase spectral weight in the region where additional Higgs spectral weight is present. (i): The Higgs threshold ω_{higgs}, the speed of sound c_s and the two particle continuum threshold $2E_{gap}$ (pair-breaking scale) as a function of V/t. (j)-(l): The density plot of amplitude-phase cross-correlator $P_{12} + P_{21}$ for (j) $V/t = 1$, (k) $V/t = 3$, and (l) $V/t = 6$. The mixing term grows in magnitude but oscillates in sign more rapidly as disorder is increased leading to cancellations in measurable response functions. Here, we present data with $U/t = 3$ on a 24×24 lattice, at an average fermion density $\rho = 0.875$, and averaged over 15 disorder realizations.

tor, there is a single collective mode in the system. While the eigenfunction is a pure phase mode at $q = 0$, it has a mixture of amplitude (Higgs) and phase components at finite q. This is also seen from Fig. 2(a) and (e) for the clean case ($V/t = 0$). However, the maximum fraction of the Higgs mode for any q at $U = 3$ is only $\sim 2\%$, which is very small. We first note that at weak disorder ($V/t = 0.1$) in Fig. 2 (f), the phase mode does not have any weight near $q = [0, 0]$ around $\omega/t \sim 1.0$, where the Higgs mode has substantial weight. The linearly dispersing collective mode (the Goldstone mode) at low q broadens with disorder, and the dispersion becomes flatter. But unlike the amplitude sector, the dispersive mode can be identified even for large disorder $V/t \approx 5$. The speed of sound, extracted from the slope of the dispersion (Fig. 2 (i)) decreases with disorder, going to zero near $V/t \approx 5.5$. It is also evident from the color-scales that phase fluctuations dominate over amplitude fluctuations in the entire disorder range.

Finally, in Fig. 2 (j)-(l), we plot the mixing term $P_{12}(q, \omega) + P_{21}(q, \omega)$ for increasing disorder. With increasing disorder the mixing term rapidly oscillates in sign as a function of frequency, thereby contributing only small corrections to the pair spectral function.

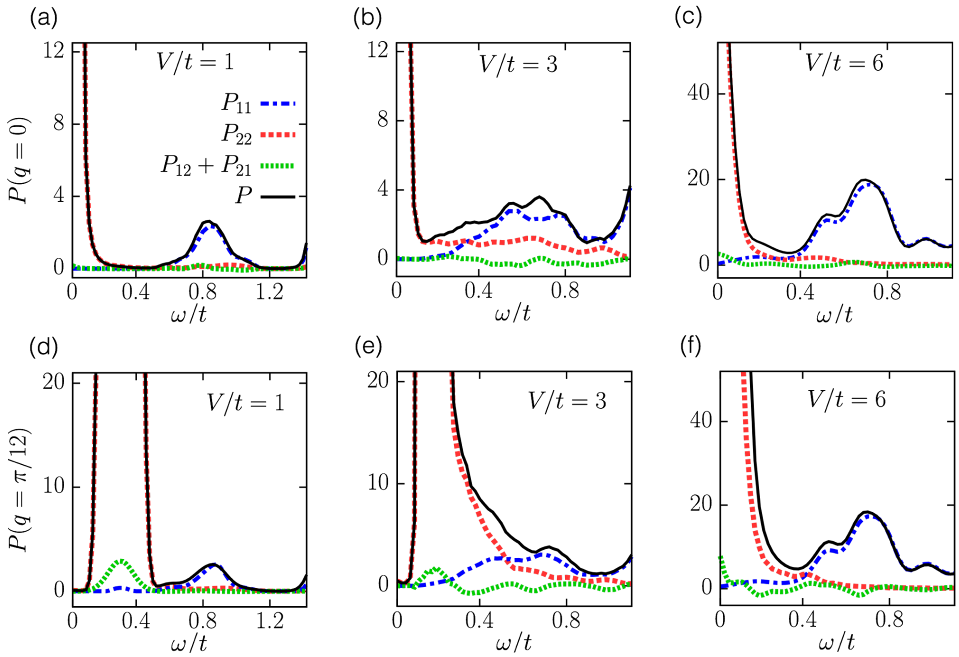

FIG. 3. Energy dependence of the spectral function at low q, (a)-(c): $P(q = [0, 0], \omega)$ and (d)-(f): $P(q = [\pi/12, 0], \omega)$ for increasing disorder $V/t = 1$, $V/t = 3$, and $V/t = 6$. The decomposition of the contributions from the Higgs mode P_{11}, phase mode P_{22} and the mixing $P_{12} + P_{21}$ is also shown. Note the negligible mixing contributions, and the spectral separation of Higgs and phase contributions. The mixing term is weaker than the Higgs weight, and both are much smaller than the weight in the phase mode. Here, we present data with $U/t = 3$ on a 24×24 lattice, at an average fermion density $\rho = 0.875$.

In case of the frequency integrated local spectral function (Fig. 1 (e)), we have shown that it is dominated by the phase fluctuations. On the other hand, in $q - \omega$ space also, the spectral function is seen to be dominated by the phase mode for most of the q and ω values (Fig. 2 (a)-(h)). The clear dominance of the phase modes over Higgs modes leads to the question whether the interesting features of the Higgs spectral function can be visible in experiments. Fortunately, the features of the Higgs and the phase spectral functions are well separated in energy at low q and hence probes which couple to the spatially averaged pair spectral function in a energy resolved manner should see these features clearly. In Fig. 3 (a)-(c), we plot $P(q = [0, 0], \omega)$ as a function of ω and we show that for all disorder the Higgs spectral weight is well separated from the low energy phase pile-up. We also present data for the smallest possible q value, i.e. $q = [\pi/12, 0]$ in Fig. 3 (d)-(f) and we show that the above features are not special for $q = 0$, but they are also true for small q values. Hence, we conclude that the probes which couple to the spatially averaged pair spectral function in an energy resolved manner should see these features clearly.

This spectral separation is a feature of low q response and is not present in the local response we investigated in the previous section. In contrast, in Ref. 11, the $q = 0$ spectral weight in Higgs and phase modes were found to overlap in energy. The difference arises as low energy density fluctuations are integrated out in Ref. 11 within a modified Random Phase Approximation (RPA), which leads to broadening of the Higgs spectral function. We also note that the spectral separation of the Higgs weight from phase is not special to $q = 0$, and holds true for low momenta (e.g. $q = [\pi/12, 0]$ shown in Fig. 3 (d)-(f)).

We also find that the amplitude-phase mixing term has negligible contribution at all frequencies near $q = 0$, and the relative contribution decreases with disorder, contrary to the popular belief that they are the dominant force in shaping the collective spectrum. This can be understood from the fact that the mixing contribution varies from positive to negative values in space, as seen in Fig. 1 (f), and hence averages to zero when one looks at low q response of the system. Our results provide guidance for momentum and energy resolved M-EELS measurements[28] to observe the Higgs and Goldstone modes as well as for scanning Josephson spectroscopy to observe the local superconducting order parameter in disordered superconductors close to the quantum phase transition.

V. CONCLUSION

We have investigated the evolution of collective modes in a disordered s-wave superconductor starting from a microscopic description. In presence of disorder, the single particle fermionic spectrum remains gapped and hence the fluctuations of the local superconducting order parameter (the phase or Goldstone mode and the amplitude or Higgs mode) are the key low energy excitations which drive the superfluid-insulator transition (SIT). We investigate the behavior of these excitations both in real and in momentum space thereby providing complimentary information relevant for different experimental probes. We find that the local low energy 2-particle spectral weight is strongly correlated with the superconducting regions and strongly anti-correlated with regions of high one particle spectral gap. The anti-correlation increases with disorder. The pair response is dominated by the phase mode, but the Higgs mode shows interesting features at low q which are spectrally separated from the phase mode contributions. The amplitude-phase mixing term oscillates with rapid change of sign both in space and in frequency, and hence its contribution is expected to play a subdominant role in most experiments which coarse grain either over space or over frequency.

Acknowledgments: The authors thank P. Raychaudhuri for useful discussions. A.S., A.R. and R.S. acknowledge computational facilities at the Department of Theoretical Physics, TIFR Mumbai. N.T. acknowledges funding from grant NSF-DMR-1309461.

Appendix A: Connection between saddle point and BdG

To see the connection between the saddle point of the fermionic action (Eqn. 3) and BdG theory, it is instructive to note that in the Matsubara frequency domain ($i\omega_n = 2\pi i/\beta$) the saddle point inverse Green's function G_0^{-1} is related to the BdG Hamiltonian[5], H_{BdG} through

$$G_0^{-1}(r, r', \omega_n) = i\omega_n \mathbb{I} - H_{BdG}. \tag{A1}$$

Let Γ be the unitary transform that diagonalizes the BdG matrix. If the eigenvalues of the matrix are given by E_α and corresponding eigenvectors are $[u_\alpha(r), v_\alpha(r)]$, then

$$\Gamma^\dagger H_{BdG} \Gamma = E_\alpha \delta_{\alpha\gamma} \tag{A2}$$

where the matrix Γ is formed by the column of eigenvectors, i.e. $\Gamma_{r\alpha} = u_\alpha(r)$ if $r < N_s$ and $\Gamma_{r\alpha} = v_\alpha(r)$ if $r \geq N_s$. The particle-hole symmetry of the BdG Hamiltonian implies that eigenvalues come in pairs of $(E_\alpha, -E_\alpha)$ and if $[u_\alpha(r), v_\alpha(r)]$ is the eigenvector corresponding to E_α, the eigenvector corresponding to $-E_\alpha$ is given by $[-v_\alpha^*(r), u_\alpha^*(r)]$.

To obtain the saddle point equation, we integrate out the fermions to obtain the saddle point action (S_0), which is given by

$$S_0 = \frac{\beta}{U}(|\Delta_0(r)|^2 + \xi_0(r)^2) - \sum_{\omega_n} Tr ln G_0^{-1}(r, r', \omega_n) \tag{A3}$$

where the Trace is over Nambu and site indices. Using $\partial S_0/\partial \Delta_0^*(r) = 0$, we get

$$\begin{aligned}
\Delta_0(r) &= \frac{U}{\beta}\sum_{\omega_n} Tr\left[G_0(\omega_n)\frac{\partial G_0^{-1}(\omega_n)}{\partial \Delta_0^*(r)}\right] \\
&= \frac{U}{\beta}\sum_{\omega_n} Tr\left[\Gamma^\dagger G_0(\omega_n)\Gamma\Gamma^\dagger \frac{\partial G_0^{-1}(\omega_n)}{\partial \Delta_0^*(r)}\Gamma\right] \\
&= \frac{U}{\beta}\sum_{\omega_n}\sum_{\alpha} \frac{\left[\Gamma^\dagger \frac{\partial G_0^{-1}(\omega_n)}{\partial \Delta_0^*(r)}\Gamma\right]_{\alpha\alpha}}{r\omega_n - E_\alpha}
\end{aligned} \tag{A4}$$

where we have used the fact that trace is invariant under unitary transforms. Using $\partial G_0^{-1}(\omega_n)/\partial \Delta_0^*(r) = -\delta_{rr'}\sigma^-$, we get the numerator to be $-\Gamma^\dagger_{r,\alpha}\Gamma_{r+N_s,\alpha} = -u_\alpha^*(r)v_\alpha(r)$. So we get

$$\begin{aligned}
\Delta_0(r) &= -\frac{U}{\beta}\sum_{\alpha}\sum_{\omega_n} \frac{u_\alpha^*(r)v_\alpha(r)}{i\omega_n - E_\alpha} \\
&= -U\sum_{\alpha} u_\alpha^*(r)v_\alpha(r)n_F(E_\alpha) \\
&= U\sum_{E_\alpha > 0} u_\alpha^*(r)v_\alpha(r)\tanh(E_\alpha/2T).
\end{aligned} \tag{A5}$$

where $n_F(E_\alpha)$ is the Fermi distribution function at temperature T. At $T = 0$, we get back the self-consistency equation for $\Delta_0(r)$ (Eqn. 6). Similarly we can also derive the self-consistency equation for $\xi_0(r)$ (Eqn. 7) from $\delta S_0/\delta \xi_0(r) = 0$.

Appendix B: Comparison of our method with other approaches

We now discuss our method in the context of other approaches used to study strongly disordered superconductors. The BdG inhomogeneous mean field theory shows evidence for formation of superconducting and non-superconducting patches in a strongly disordered superconductor[5]. At the expense of numerically solving a large number of self-consistency equations, this method treats disorder exactly. This forms the starting point of our calculation.

The gaussian fluctuations around the inhomogeneous saddle point has been studied previously in Ref.[11] with a focus on the $q = 0$ spectral function. However, there is a key technical difference between Ref.[11] and our work. In both approaches, the action is expanded to quadratic order in fluctuations around the saddle point; however, in Ref.[11], the fluctuations of the local density field $\xi(r, \tau)$ is considered as an independent field, leading to a 3×3 fluctuation propagator. The ξ fields are then integrated out to obtain a renormalized 2×2 propagator. Here the density and phase fields are treated independently, even though, in principle, these fields should be related by the number-phase uncertainty relation. Another reason to question the validity of integrating out density fluctuations is that, unlike the gapped fermions, the density fluctuations have low energy weight in the same range as the Higgs and the phase fluctuations, and integrating them out while

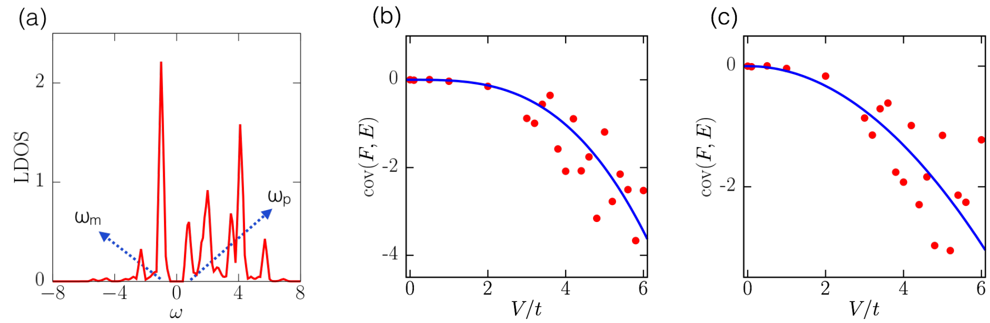

FIG. 4. (a): LDOS as a function of ω for a particular site. The locations of ω_p and ω_m are indicated in the figure. (b)-(c): Covariance between two particle spectral function (F) and local single particle gap (E) where F is defined as (b) $F(r) = \frac{1}{0.8\times 2E_{gap}} \int_{0.2\times 2E_{gap}}^{2E_{gap}} d\omega P(r,r,\omega)$ and (c) $F(r) = \frac{1}{0.7\times 2E_{gap}} \int_{0.3\times 2E_{gap}}^{2E_{gap}} d\omega P(r,r,\omega)$.

keeping the Higgs and phase fluctuations is an uncontrolled procedure. The direct consequence of integrating out the soft modes is a strong broadening of the Higgs spectral function in Ref. [11], resulting in the overlap of the Higgs and phase spectral weights. In contrast, our approach fixes the ξ fields to their saddle point value that results in spectrally separated Higgs and phase modes at $q = 0$.

Finally the superconductor-insulator transition has also been studied with Monte Carlo techniques[6], which include the vortex excitations missed in calculations that retain only Gaussian fluctuations. However, QMC is limited to small lattice sizes, requires analytic continuation to obtain real frequency response, and even so only provides the total response without being able to separate them into amplitude and phase components.

Appendix C: Local Single Particle Gap

In this section we provide the details of our method to obtain the local gap map, which is also used to show anti-correlation between one particle gap and two particle spectral weight in the system. The local single particle density of states (LDOS) for each site i, calculated from BdG MF theory, is given by

$$N_\omega(r) = \frac{1}{N_s}\sum_n u_n^2(r)\delta(\omega - E_n) + v_n^2(r)\delta(\omega + E_n). \quad \text{(C1)}$$

The local single particle gap $E(r)$ for each site r is obtained from $E(r) = \frac{\omega_p(r) - \omega_m(r)}{2}$, where $\omega_p(r)$ is the location of the lowest energy peak in LDOS for $\omega > 0$ and $\omega_m(r)$ is the location of the highest energy peak in LDOS for $\omega < 0$. In Fig. 4(a) we have shown a sample LDOS for a particular site. The figure also shows the location of $\omega_p(r)$ and $\omega_m(r)$ for this site and the corresponding local gap $E(r)$ obtained from this LDOS.

Appendix D: Covariance between Single Particle Gap and Two Particle Spectral Function

To understand the spatial variation for the local two particle spectral function ($P(r, r, \omega)$), we consider the integrated spectral weight of P, $F(r) = \frac{1}{2E_{gap}} \int_0^{2E_{gap}} d\omega P(r,r,\omega)$. We calculate the covariance between two experimentally observable quantities namely two particle spectral function (F) and local single particle gap (E) as

$$\mathrm{cov}(F, E) = \langle FE\rangle - \langle F\rangle\langle E\rangle. \quad \text{(D1)}$$

In Fig. 4 (b) and (c) we show the covariance between F and E as a function of disorder, where F has been calculated with different integration limits, $F(r) = \frac{1}{0.8\times 2E_{gap}} \int_{0.2\times 2E_{gap}}^{2E_{gap}} d\omega P(r,r,\omega)$ and $F(r) = \frac{1}{0.7\times 2E_{gap}} \int_{0.3\times 2E_{gap}}^{2E_{gap}} d\omega P(r,r,\omega)$ respectively. We find that with increasing the lower cut-off of the integration the anti-correlation between F and E at large disorder persists but it becomes weaker.

* abhisek@theory.tifr.res.in
† sensarma@theory.tifr.res.in

1 Lee, P. A., Nagaosa, N. & Wen, X. Doping a Mott insulator: Physics of high-temperature superconductivity. *Rev. Mod. Phys.* **78**, 17 (2006).
2 Anderson, P. W., Lee, P. A., Randeria, M., Rice, T. M., Trivedi, N. & Zhang, F. C. The physics behind high-temperature superconducting Cuprates : the 'plain vanilla' version Of RVB. *J Phys. Condens. Matter* **16**, R755 (2004).
3 Melo, C. A. R. Sa de, Randeria, M. & Engelbrecht, J. R. Crossover from BCS to Bose superconductivity : Transition temperature

and time-dependent Ginzburg-Landau Theory. *Phys. Rev. Lett.* **71**, 3202 (1993).

[4] Fisher, M. P. A., Weichman, P. B., Grinstein, G. & Fisher, D. S. Boson localization and the superfluid-insulator transition. *Phys. Rev. B* **40**, 546570 (1989).

[5] Ghosal, A., Randeria, M. & Trivedi, N. Inhomogeneous pairing in highly disordered s-wave superconductors. *Phys. Rev. B* **65**, 014501 (2001).

[6] Bouadim, K., Loh, Y. L., Randeria, M. & Trivedi, N. Single- and two-particle energy gaps across the disorder-driven superconductor-insulator transition. *Nature Physics* **7**, 884-889 (2011).

[7] Trivedi, N., Scalettar, R. T., & Randeria, M. Superconductor-insulator transition in a disordered electronic system. *Phys. Rev. B* **54**, R3756-R3759 (1996).

[8] Sherman, D. et al. The Higgs mode in disordered superconductors close to a quantum phase transition. *Nature Physics* **11**, 188-192 (2015).

[9] Mondal, M. et al. Phase fluctuations in a strongly disordered s-wave NbN superconductor close to the metal-insulator transition. *Phys. Rev. Lett.* **106**, 047001 (2011).

[10] Matsunaga, R. et al. Light-induced collective pseudospin precession resonating with Higgs mode in a superconductor. *Science* **345**, 1145-1149 (2014).

[11] Cea, T., Castellani, C., Seibold, G. & Benfatto. L. Nonrelativistic dynamics of the amplitude (Higgs) mode in superconductors. *Phys. Rev. Lett.* **115**, 157002 (2015).

[12] Cea, T. & Benfatto, L. Nature and Raman signatures of the Higgs amplitude mode in the coexisting superconducting and charge-density-wave state. *Phys. Rev. B* **90**, 224515 (2014).

[13] Goldman, A. & Markovic, N. Superconductor-insulator transitions in the two-dimensional limit. *Phys. Today* **51**, 39-44 (November, 1998).

[14] Gantmakher, V. F. & Dolgopolov, V. T. Superconductor-insulator quantum phase transition. *Phys. Usp.* **53**, 3-53 (2010).

[15] Hebard, A. F. & Paalanen, M. A. Magnetic-field-tuned superconductor-insulator transition in two-dimensional films. *Phys. Rev. Lett.* **65**, 927-930 (1990).

[16] Kemper, A. F., Sentef, M. A., Moritz, B., Freericks, J. K. & Devereaux, T. P. Direct observation of Higgs mode oscillations in the pump-probe photoemission spectra of electron-phonon mediated superconductors. *Phys. Rev. B* **92**, 224517 (2015).

[17] Measson, M.-A., Gallais, Y., Cazayous, M., Clair, B., Rodiere, P., Cario, L. & Sacuto, A. Amplitude Higgs mode in the 2H-NbSe2 superconductor, Phys. Rev. B **89**, 060503(R) (2014).

[18] Endres, M., Fukuhara, T., Pekker, D., Cheneau, M., Schauss, P., Gross, C. Demler, E., Kuhr, S. & Bloch, I. The Higgs amplitude mode at the two-dimensional superfluid/Mott insulator transition. *Nature* **487**, 454-458 (2012).

[19] Diener, R. B., Sensarma, R. & Randeria, M. Quantum fluctuations in the superfluid state of the BCS-BEC crossover. *Phys. Rev. A* **77**, 023626 (2008).

[20] Sacepe, B., Chapelier C., Baturina, T. I., Vinokur, V. M., Baklanov, M. R. & Sanquer, M. Disorder induced inhomogeneities of the superconducting state close to superconductor-insulator transition. *Phys. Rev. Lett.* **101**, 157006 (2008).

[21] Chockalingam, S. P., Chand, M., Kamlapure, A., Jesudasan, J., Mishra, A., Tripathi, V. & Raychaudhuri, P. Tunneling studies in a homogeneously disordered s-wave superconductor: NbN. *Phys. Rev. B* **79**, 094509 (2009).

[22] Randeria, M. T., Feldman, B. E., Drozdov, I. K. & Yazdani, A. Scanning Josephson Spectroscopy on atomic scale. *Phys. Rev. B* **93**, 161115(R) (2016).

[23] Sachdev, S. *Quantum Phase Transitions* (Cambridge Univ. Press, 2001).

[24] We note that our formalism calculates the correlators in real frequencies analytically and does not suffer from issues of analytic continuation.

[25] Kim, Y. B. & Wen, X-G. Effects of collective modes on pair tunneling into superconductors. *Phys. Rev. B* **48**, 6319 (1993).

[26] Gazit, S., Podolsky, D. & Auerbach, A. Fate of the Higgs mode near quantum criticality. *Phys. Rev. Lett.* **110**, 140401 (2013).

[27] Cheng, B., Wu, L., Laurita, N. J., Singh, H., Chand, M., Raychaudhuri, P. & Armitage, N. P. Anomalous gap-edge dissipation in disordered superconductors on the brink of localization. *Phys. Rev. B* **93**, 180511 (2016).

[28] Kogar, A., Rak, M. S., Vig, S., Husain, A. A., Flicker, F., Joe, Y., Luc Venema, MacDougall, G. J., Chiang, T. C., Fradkin, E., Wezel J. V. & Abbamonte, P. Signatures of exciton condensation in a transition metal dichalcogenide. *Science* **358**, 1314-1317 (2017).